Changes in extreme high water levels based on a quasi-global tide-gauge data set

Melisa Menéndez[1] and Philip L. Woodworth[2]

Received 19 November 2009; revised 15 April 2010; accepted 2 June 2010; published 8 October 2010.

[1] A quasi-global sea level data set from tide gauges has been used to investigate extreme sea level events and their spatial and temporal variabilities. Modern methods based on a nonstationary extreme value analysis have been applied to the maxima of the total elevations and surges for the period of 1970 and onward. A subset of the data was used to study changes over the 20th century. The analyses demonstrate the magnitude and timing of the seasonal cycle of extreme sea level occurrence, the magnitude of long-term trends in extreme sea levels, the evidence for perigean and nodal astronomical tidal components in the extremes, and the relationship of the interannual variability in high water levels to other ocean and atmosphere variations as represented by climate indices. The subtraction from the extreme sea levels of the corresponding annual median sea level results in a reduction in the magnitude of trends at most stations, leading to the conclusion that much of the change in the extremes is due to change in the mean values.

Citation: Menéndez, M., and P. L. Woodworth (2010), Changes in extreme high water levels based on a quasi-global tide-gauge data set, *J. Geophys. Res.*, *115*, C10011, doi:10.1029/2009JC005997.

1. Introduction

[2] Extreme sea level events have immediate and obvious impacts on the coast, unlike changes in mean sea level which are much longer term. The recent occurrence of major floods in hurricanes Katrina, Sidr, and Nargis have emphasized the damage that storm surges are capable of, especially when combined with the rise in coastal populations. Although the evidence for recent increases in the frequency and magnitude of extreme events is mixed, there is an obvious requirement to learn more about the statistics of extreme sea level events and of surges, partly as input to studies of extremes which might occur in the future.

[3] The observed sea level can be considered as a combination of four factors: mean sea level, tide, surge, and waves. Waves are averaged out in most sea level records obtained from tide gauges, which tend to have samplings of several minutes up to an hour, and so we do not discuss their contribution to the overall sea level signal further in the present study.

[4] Mean sea level (MSL) is the average level of the sea over a stated period relative to a fixed benchmark on land near to the tide gauge. MSL has generally increased worldwide during the 20th century due to the thermal expansion of sea water, the melting of ice sheets and glaciers, and the hydrological exchanges between the land and the ocean [*Bindoff et al.*, 2007]. However, there are many locations where the MSL (i.e., relative to land) is falling because the land upon which the gauge is situated is rising [e.g., *Peltier*, 2001]. High tidal levels contribute to the occurrence of extreme high water levels. Astronomical modulations such as the equinoctal spring tides, the interannual perigean influence, or the nodal cycle can increase the risk of flooding at specific times [*Pugh*, 1987]. Storm surges are the result of low air pressures and the effect of wind stress in shallow-water areas. Higher surge values are associated with both midlatitude and tropical storms, although the most intense cyclones are not necessarily associated with the largest coastal surges. Interactions between the tide and surge may be important in some coastal areas, resulting in a modification of the surge height, depending on tide level. Changes in storminess and MSL, each of them a consequence of climate change, may have an important combined role in modifying the frequency and magnitude of extreme sea levels.

[5] Currently, there are two main approaches to study the climate variability of sea levels: studying the past and modeling the future. The former makes a revision of historical data sets based on instrumental measurements or numerical modeling. This approach can include estimations of trends in extremes and correlations with other regional climate parameters. Sophisticated extreme value analyses are also able to forecast future extreme values [i.e., *Menéndez et al.*, 2009b; *Wang and Zhang*, 2008]. The second approach is based on projections of future sea level elevations derived from meteorological fields extracted from atmosphere-ocean general circulation models [e.g., *Lowe et al.*, 2001]. In the present study, we confine ourselves to a study of historical data.

[1]Environmental Hydraulic Institute, E.T.S. Ingenieros de Caminos, Canales y Puertos, Universidad de Cantabria, Santander, Spain.
[2]Proudman Oceanographic Laboratory, Liverpool, UK.

0148-0227/10/2009JC005997

[6] A number of studies have analyzed changes in historical extreme high water levels, although most of them have concentrated on a specific location or region and used different methods and measurement epochs [*Lowe et al.*, 2010]. Several of these studies concluded that there is evidence for an increase over time of high water levels [e.g., *Araújo and Pugh*, 2008, for Newlyn and Brest; *Méndez et al.*, 2007, for San Francisco]. The only investigation which has attempted a quasi-global investigation is that of *Woodworth and Blackman* [2004], who employed a tide gauge data set similar to, but smaller than, that of the present study.

[7] Many studies have investigated whether extreme values are changing in a significantly different way to MSL. *Zhang et al.* [2000] concluded that there was no discernible increase in modern storms over the U.S. West Coast during the last century and that the flooding has been exacerbated by the effect of the MSL rise. *Bernier and Thompson* [2006] observed a small reduction in extreme events in the northwest Atlantic between 1960 and 1999 because of changes in atmospheric conditions. The lack of trends in the nontidal sea level variability around the United Kingdom was noted by *Pugh and Maul* [1999] over the last century. In the Mediterranean, a decrease of strong positive surges in the northern Adriatic was detected by *Raicich* [2003] and *Marcos et al.* [2009]. *Bromirski et al.* [2003] found a substantial increasing trend in winter extreme surges at San Francisco since about 1950. *Church et al.* [2006] observed an increase in the frequency of high water levels (storm surges plus MSL rise) to the post-1950 period for two tide gauges on the east and west Australian coasts, consistent with increased regional coastal flooding.

[8] This paper investigates the worldwide patterns of historical extreme sea level changes by means of an extreme value analysis applied to a quasi-global sea level data set. The paper is organized as follow. In section 2, the tide gauge data set is briefly described. In section 3, we describe the nonstationary extreme statistical approach. The different time scale variations are measured statistically using a time-dependent generalized extreme value distribution and a nonhomogeneous Poisson process. Section 4 provides a discussion of the month within a year that presents more probability for a high water level, trends in high water levels and storm surges, and explores the relationship of ocean and atmospheric variability. The question of whether there is a different behavior in extremes over and above the much-studied MSL variability is also examined. Finally, in section 5 we present some concluding comments.

2. Sea Level Data Set

[9] This work makes use of the Global Extreme Sea Level Analysis (GESLA) quasi-global tide gauge data set which has been collected by the Antarctic Climate and Ecosystems Cooperative Research Centre (ACE CRC) and the Proudman Oceanographic Laboratory. The present version of the data set consists of 675 separate sea level records, the majority of them coming from the archives of the University of Hawaii Sea Level Center (data available at http://uhslc.soest.hawaii.edu) and the Global Sea Level Observing System (data available at www.gloss-sealevel.org). Other records were obtained from a number of national data centers.

[10] The data set required preprocessing. It contains duplicate records, jumps in datum, obvious outliers, and different sampling intervals, even within the same station records. Jumps in datum were corrected by assessing the difference in the mean for similar time spans and outliers were removed. Hourly values, which comprise the most usual sampling, have been selected by subsampling any higher frequency data.

[11] Once the GESLA data set was preprocessed, two periods of time were analyzed: the period of 1970 onward, to study variability in recent decades (we have chosen stations to have at least 15 years of sea level data), and records with at least 60 years of sea level data, which give us information about variations during the last century. Figure 1 shows the geographical distribution of the whole GESLA data set and the selected stations for the extreme value analyses (258 for the study of variability in recent decades and 49 for estimating long-term variations).

[12] The GESLA data set has a worldwide spatial distribution. However, the Southern Hemisphere has poorer geographical coverage than the Northern Hemisphere and shorter records. It provides poor coverage for stations with data after 1970 in the Indian Ocean and limited scope for study of longer records in the Southern Hemisphere.

[13] Two variables are examined in this work: the total sea level elevation for each station and the surge component. The analysis of the total sea level variable provides valuable information on flooding risk, while information on surges provides insight into changes in storm activity.

[14] The tidal component was subtracted from each station record in order to obtain the residual signal. The residuals were obtained by subjecting two consecutive years of data to a tidal analysis with the use of the Tidal Analysis Software Kit (TASK) (TASK data available at www.psmsl.org/train_and_info/software/task2K.php) and with a standard set of 63 harmonic constituents. The residuals for the middle 12 months of each set of two calendar years of data were selected; the MSL and its seasonal cycle having been defined separately within the tidal analysis. In this case, the residual signal can be considered as a "surge" component.

3. Methodology

[15] The approaches to study variations in extreme sea level events can be thought of as either changes in the magnitude of the higher water level events or, alternatively, changes on the occurrence of these extreme events. An approach based on magnitude allows for the estimation of the water levels associated with high-return periods and makes use of more information about the extreme sea level events than in the frequency analysis. The frequency approach makes use of only the timing of extreme sea level events and avoids the possible errors in height of the higher water level measurements. Here, two models are proposed to study changes in extreme high water levels: a time-dependent generalized extreme value distribution (GEVD) and a nonhomogeneous Poisson process. The maximum likelihood method is used to fit these models [*Coles*, 2001; *Castillo et al.*, 2005].

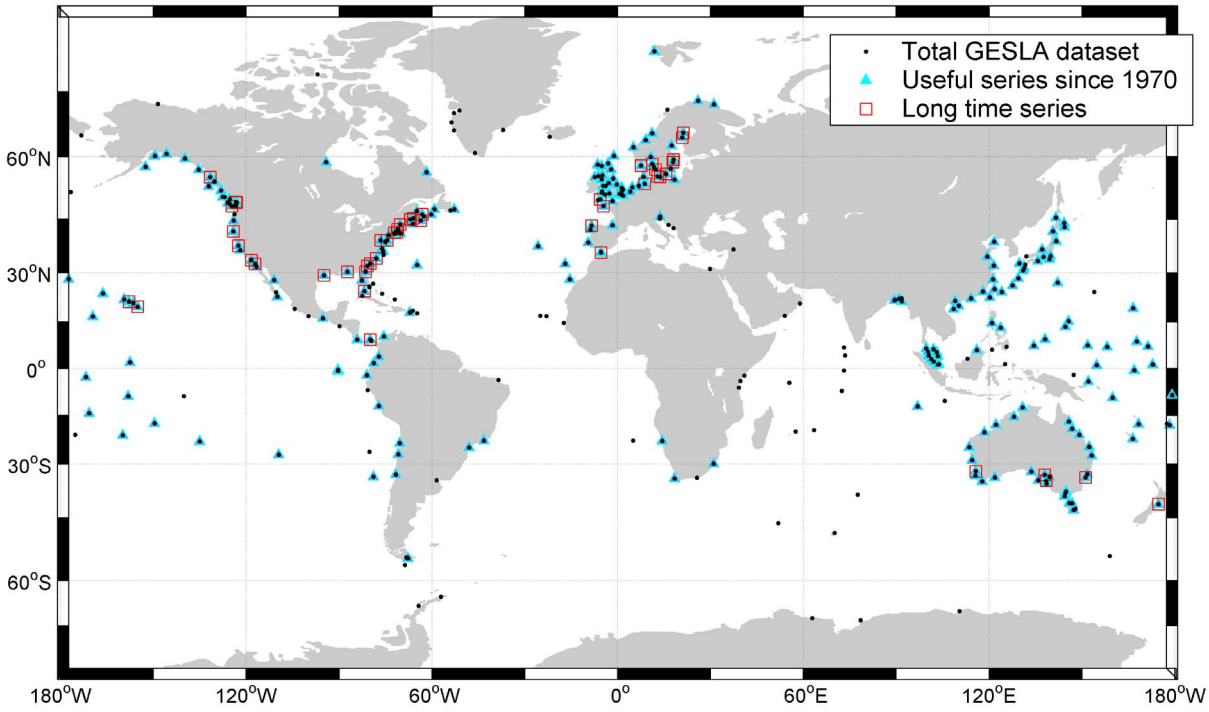

Figure 1. Location of tide gauges in the Global Extreme Sea Level Analysis (GESLA) data set.

3.1. Selection of Extreme Values

[16] Several possible techniques have been used to characterize extreme sea level events: high annual percentiles [e.g., *Woodworth and Blackman*, 2004], maxima in a block of time [e.g., *Araújo and Pugh*, 2008; *Méndez et al.*, 2007], maxima of *r* events per year [e.g., *Marcos et al.*, 2009], and the peaks over a certain threshold [*Zhang et al.*, 2000]. The use of high percentiles solves the problem of a possible bias in annual maxima due to incorrectly measured hourly values [*Woodworth and Blackman*, 2002], but it is not possible to use them for the estimation of high water levels associated with return periods. The main difficulties with the annual maxima method (the simplest and most widely used in extreme analysis) are to do with data incompleteness and not taking into account the possibility of several extreme events within a year. The latter is solved by the methods which select shorter time blocks than a year, the *r*-largest values within a year, or the maximum values over a threshold.

[17] The method used here makes use of monthly maxima (MM). In the present analysis, gaps summing to more than 40% of the hourly values for a given month invalidate the use of this monthly maximum. The MM method solves the problem of strong biasing in annual values if the record contains occasional data gaps, and modeling the seasonal dependence is essential for a good estimation of high-return periods.

[18] Although tide and surge are major components of the sea surface record, variations due to mean sea level rise, crustal motions, and local geographical changes may also be represented in the total elevations. Following *Woodworth and Blackman* [2004], in order to investigate any climate variability in extreme sea level over and above changes in MSL, the annual median of the hourly values has been subtracted from each MM. The monthly maxima with the annual median reduced (MM_R) are not then affected by vertical land movements and datum uncertainties. A comparison of climate variability between the MM of total elevations and MM_R might inform us whether the variability of the most severe sea level events is similar to that in the MSL.

[19] On the other hand, extreme sea levels may not always arise from high tide levels combined with extreme surges. Sometimes, they may be determined primarily by extreme tides and moderate surges, whereas in other cases, it is primarily the extreme surges in combination with moderate tides that are important. Even in cases when surge is the predominant factor in high water levels, there may be a nonlinear interaction between the surge and tide that may cause a maximum residual at a time offset from the overall high water level [*Horsburgh and Wilson*, 2007]. Because surge maxima are of great interest in climate research with regard to possible changes in the frequency and magnitude of storms, and as they are of potential importance to flood risk if they occur at high tide, the MM of surge have also been analyzed.

[20] The timing of the higher extreme sea level events for the frequency analysis has been defined by the peak over threshold (POT) technique. The threshold has to be high enough to ensure that exceedances describe real extreme events. In the present analysis, the threshold for each station has been set at the 99.5 percentile of the complete record. A time span of five days has been required between successive events to ensure independence between events. An average of four to five extreme events per year is found in this way for the majority of stations.

3.2. Statistical Approach

3.2.1. GEVD Model

[21] The justification for using the GEVD is that it corresponds to the class of all possible limiting distributions for maxima. Moreover, the POT approach converges to the GEVD [*Pickands*, 1975]. The three-parameter cumulative distribution function of the GEVD is given by

$$F_t(z) = \begin{cases} \exp\left\{-\left[1+\xi\left(\frac{z-\mu(t)}{\psi(t)}\right)\right]_+^{-1/\xi}\right\} & \xi \neq 0 \\ \exp\left\{-\exp\left[-\left(\frac{z-\mu(t)}{\psi(t)}\right)\right]\right\} & \xi = 0, \end{cases} \quad (1)$$

where $[a]_+ = \max[a, 0]$, μ is the location parameter, $\psi > 0$ is the scale parameter, and ξ is the shape parameter. The GEVD includes three distribution families corresponding to the different types of the tail behavior: the Gumbel family, the Fréchet distribution, and the Weibull family.

[22] Note that GEVD has a time-dependent location $\mu(t)$ and scale parameter, $\psi(t) > 0$. The extension for nonstationary implies that the properties of the statistical distribution change through time. Therefore, the probability of a certain extreme high water level (or surge) may be larger in winter (variations within a year), in a strong El Niño year (interannual variations), or in the future (in the case of a secular increase).

[23] For nonstationary or time-dependent GEVD, the calculation of time-dependent return-level quantiles $z_R(t, \theta)$ associated with the return period R (in years) can be carried out by using

$$\begin{aligned} Z_R(t,\theta) &= Z_R(\mu(t),\psi(t),\xi) \\ &= \begin{cases} \mu(t) - \frac{\psi(t)}{\xi}\left[1-\{-\log(1-1/R)\}^{-\xi}\right] & \xi(t) \neq 0 \\ \mu(t) - \psi(t)\log\{-\log(1-1/R)\} & \xi(t) = 0. \end{cases} \end{aligned} \quad (2)$$

The estimation of the return sea level quantile $\bar{z}_R$ for a certain year t_i is obtained by solving

$$1 - 1/R = \begin{cases} \exp\left\{-\int_{t_i}^{t_i+T}[1+\xi(\bar{z}_R-\mu(t))/\psi(t)]_+^{-1/\xi}dt\right\} \\ \exp\left\{-\int_{t_i}^{t_i+T}\exp[(\mu(t)-\bar{z}_R)/\psi(t)]dt\right\}, \end{cases} \quad (3)$$

where T is one year.

3.2.2. Nonhomogeneous Poisson Process

[24] Assuming that the extreme high water level events are statistically independent of each other, their frequencies can be estimated using nonhomogeneous Poisson processes. Under the Poisson hypothesis, the cumulative distribution function of the time t_i at which the ith event occurs conditioned by the time t_{i-1} of the previous event is given by

$$F(t_i|t_{i-1}) = 1 - \exp\left[-\int_{t_{i-1}}^{t_i} v(t)dt\right], \quad (4)$$

where $v(t)$ is the occurrence rate. Note that $v(t)$ is a function of time. It implies that the number of events in a time span (e.g., one year) is not the same through time.

3.2.3. Seasonal Dependence

[25] Mean sea level seasonal oscillations have been widely studied [e.g., *Tsimplis and Woodworth*, 1994]. This variability is due to local meteorological, oceanographic, and hydrological forcings. In general, the seasonal dependence in extreme sea levels is mainly caused by astronomical (spring tides) and meteorological (storminess season) components, although a runoff component can be important in some locations [e.g., *Singh*, 2001; *Kang et al.*, 2008].

[26] The importance of seasonal variations in extreme statistical analysis of climate parameters has been noted previously. *Carter and Challenor* [1981] demonstrated, using independent monthly extreme distributions of wave heights, that the probability of the occurrence of an extreme wave height changes within the year, while *Katz et al.* [2002] obtained a better fit to the data, assuming that the annual maximum of daily precipitation depends on a particular day within a year.

[27] In this approach, the seasonal variability is explicitly modeled by the possibility of annual and semiannual cycles in the location and scale parameters. Mathematically, these seasonal cycles are included through sinusoidal functions:

$$\begin{aligned} \mu_S(t) &= \beta_0 + \sum_{i=1}^{2}[\beta_{2i-1}\cos(i\omega t) + \beta_{2i}\sin(i\omega t)] \\ \psi_S(t) &= \alpha_0 + \sum_{i=1}^{2}[\alpha_{2i-1}\cos(i\omega t) + \alpha_{2i}\sin(i\omega t)], \end{aligned} \quad (5)$$

where β_0 and α_0 are averaged values, β_i and α_i are the amplitudes of the harmonics, $\omega = 2\pi$ years^{-1}, and time t is given in years.

[28] In order to find the simplest model with a minimum number of time-dependent parameters, we employ a stepwise procedure evaluating the final prediction error (FPE) criterion [*Akaike*, 1973; *Menéndez et al.*, 2009a].

$$FPE = -2\hat{\ell}(p) + n\log\left(\frac{n+p}{n-p}\right), \quad (6)$$

where $\hat{\ell}$ is the log likelihood function (logarithm of joint probability density function for the sample of MM), n is the number of MM, and p is the number of parameters.

[29] The stepwise algorithm starts with a stationary model and tests the incorporation of seasonal cycles by evaluating the FPE criterion. Only significant sinusoidal functions (equation (5)) are hence included into the optimal model for each station (see *Menéndez et al.* [2009a] for more details). Standard likelihood theory is used to obtain the model parameter estimates $\hat{\beta}_i$, $\hat{\alpha}_i$ [*Coles*, 2001].

3.2.4. Interannual Variations and Long-Term Trends

[30] Interannual and decadal fluctuations are also present in extreme sea levels. This variability may be dependent on regional climate patterns which are often represented by teleconnection indices. The main coupled ocean-atmosphere modes affecting climate anomalies on a large regional scale are the El Niño-Southern Oscillation (ENSO) and the North Atlantic Oscillation (NAO), but many other climate modes have been used to describe climate variability.

[31] Eight relevant climate indices have been selected to investigate teleconnections in extreme high waters changes:

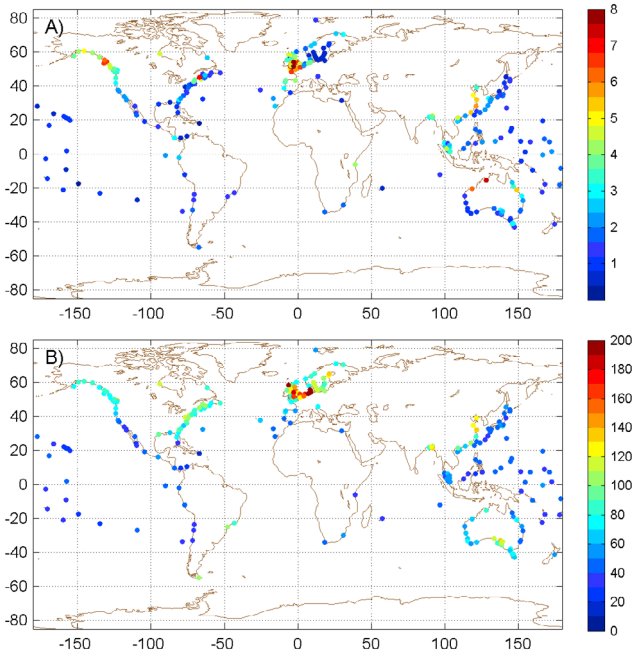

Figure 2. (a) Tidal range in meters and (b) nontidal residual range, in centimeters.

Niño3, which is the main descriptor of ENSO; NAO, which is the major mode in the North Atlantic [*Jones et al.*, 1997]; the Arctic Oscillation (AO); the Antarctic Oscillation (AAO); the Indian Ocean Dipole (IOD); the East Atlantic Oscillation (EA); the East Atlantic/Western Russian Oscillation (EAWR); the Scandinavian index (SCA), and the Pacific-North America Index (PNA). Indices that inform about decadal fluctuations (e.g., the Pacific Decadal Oscillation, PDO) are not considered, because we are studying climate variability primarily from the perspective of the past four decades. AAO was selected from the British Antarctic Survey (data available at http://www.nerc-bas.ac.uk/icd/gjma/sam.html), IOD was selected from the Japan Agency for Marine-Earth Science and Technology (data available at http://www.jamstec.go.jp), NAO was selected from the Climate Research Unit of the University of East Anglia (data available at http://www.cru.uea.ac.uk/cru), and the rest of the climate indices were selected from the National Oceanic and Atmospheric Administration-National Weather Service (data available at http://www.cpc.ncep.noaa.gov).

[32] AO and AAO, also called the annular modes, are the most important patterns of climate variability in the Northern and Southern Hemispheres. The AO has a similar pattern in the Atlantic to the NAO, but it covers more of the Arctic and North Pacific, and AAO describes the strength of the westerly winds in the Southern Ocean. The IOD has a

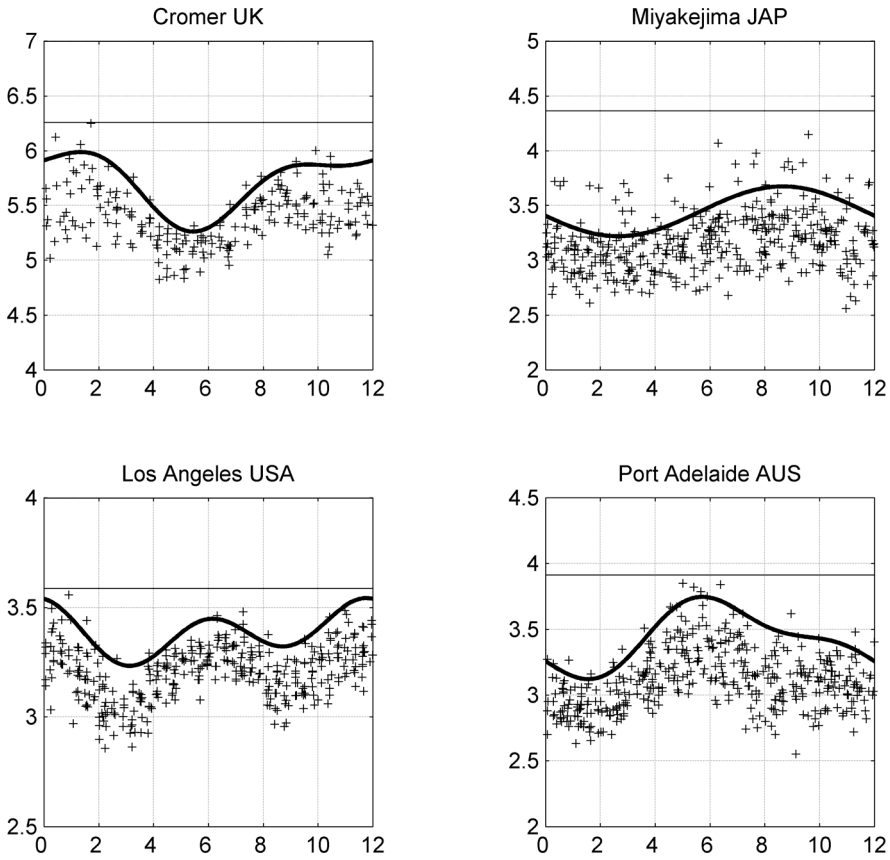

Figure 3. Model results of seasonality for four stations. Crosses represent the monthly maxima (meters), thick lines represent the 50 year time-dependent quantile, and the horizontal line represents the estimated 50 year annual return level. UK, United Kingdom; JAP, Japan; USA, United States; AUS, Australia.

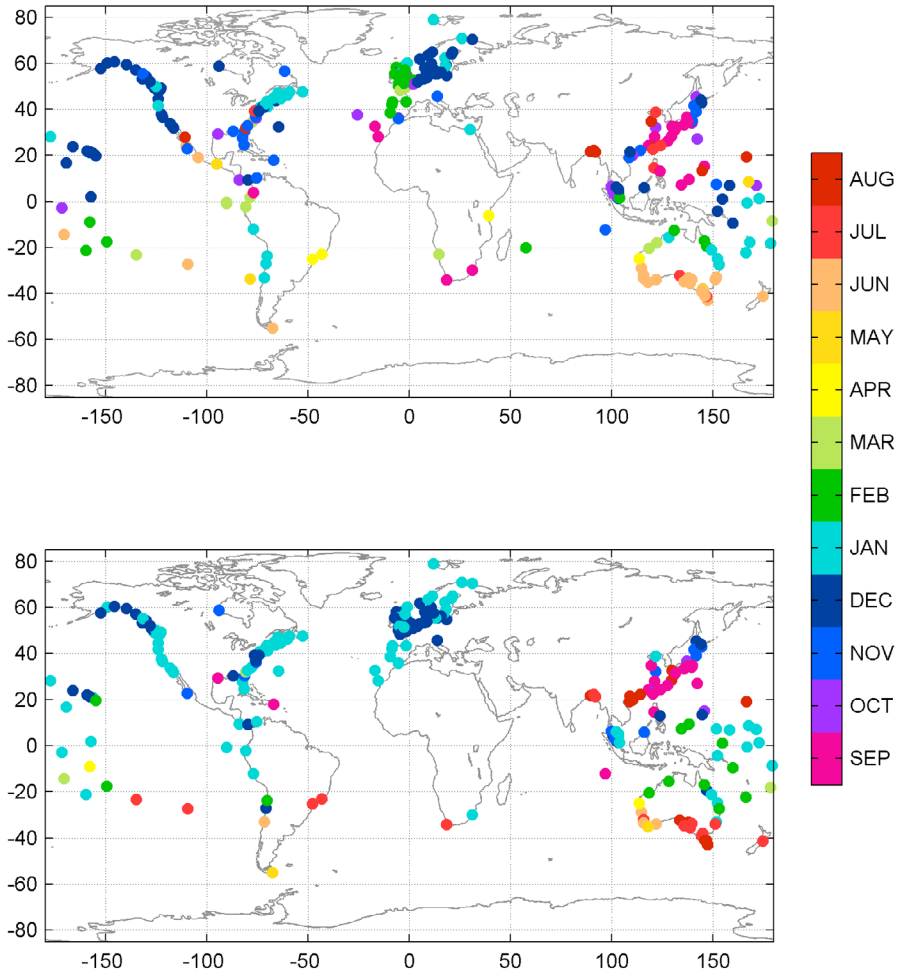

Figure 4. (Top) Month of highest water level and (bottom) month of highest nontidal residual level.

strong relation to ENSO but affects countries surrounding the Indian Ocean, especially Indonesia and Australia. EA is structurally similar to the NAO, so that these two modes appear to be interdependent. However, the lower latitude center of action of the EA contains a strong subtropical link associated with modulations in subtropical ridge intensity and location. This subtropical link makes the EA pattern distinct from its NAO counterpart. The PNA is a prominent mode in the extratropical Pacific, while the EAWR and SCA are secondary modes of climate variability in the North Atlantic. The EAWR affects Eurasia throughout the year and is also linked to eastern Asia and Northwest Canada. Finally, the SCA pattern consists of a primary circulation center that spans Scandinavia and large portions of the Arctic Ocean, north of Siberia. These indices are based on the normalized air pressure difference between specific centers, except Niño3 and IOD which are based on averaged sea surface temperatures in a region.

[33] We formulate the statistical relationship of climate indices in extreme sea levels by adding a new linear term in the location parameter of the GEVD: $\mu(t) = \mu_S(t) + \beta_{CI}\, Clim.\ Index(t)$. Thus, the parameter β_{CI} (m/unit of climate index) indicates the sensitivity of the climate pattern in the extreme sea level. The likelihood ratio test is used to estimate the significance level and confidence intervals of the climate term.

[34] A complication in interannual extreme high water level variability is the low-frequency fluctuations of ocean tides. The nodal (18.6 year) component and the quasi 4.4 year periodicity of the perigean components may be seen in the higher water levels where the tide range is large. These fluctuations are modeled using the expression $\mu(t) = \mu_S(t) + \beta_{N1}\cos(\omega t/T) + \beta_{N2}\sin(\omega t/T)$, where T is the corresponding period.

[35] To account for long-term variability, a possible trend was also included into the extreme model. Trends were computed using a linear time dependence in the location and scale parameters of the GEVD (i.e., for the location parameter, $\mu(t) = \mu_S(t) + \beta_{LT}t$). Therefore, the model is able to simulate the increase or decrease, not only in the magnitude of the extreme events, but also in their variance. The significance of each linear trend is computed by using the likelihood ratio test.

4. Results

[36] In order to obtain an idea of the spatial description in the magnitude of the tide and surge, the tidal and surge

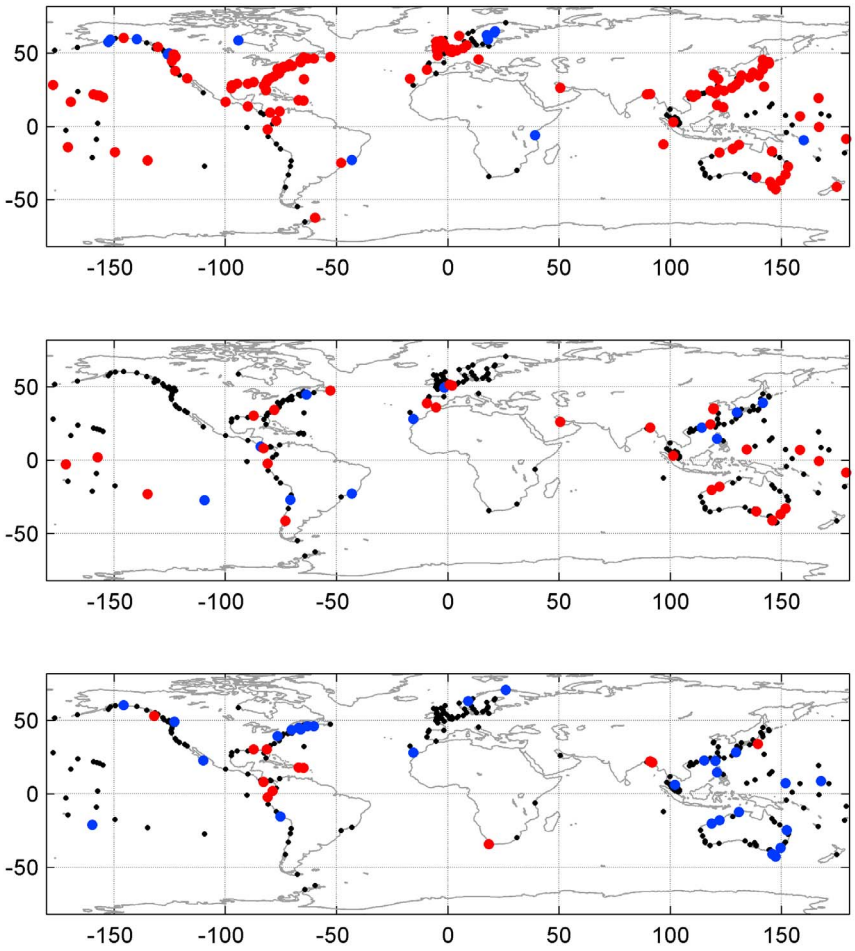

Figure 5. Estimated trends in (top) annual 99th percentile of sea level, (middle) 99th percentile reduced to medians, and (bottom) 99th percentile of the nontidal residual. Only trends at a confidence level above 95% are shown in color: red for positive trends and blue for negative trends.

ranges are displayed in Figure 2. The range was defined in terms of the difference between the 0.5 and 99.5 percentiles of each record. Tidal ranges of 5 m or more are found along the western European coast, the northwest of Australia, the Gulf of Alaska, the Bay of Fundy, and the East China Sea. Regions of higher surge contributions include northern Europe, the Chinese coast, southern Australia, the extratropical Atlantic coast of America, and the Gulf of Alaska.

4.1. Variations Within a Year

[37] Since extreme high water levels have a strong seasonal dependence, an intra-annual dependence was incorporated into the model (Figure 3). The evidence of this variation has been found previously for the San Francisco and Newlyn tide gauges [*Mendez et al.*, 2007; *Menéndez et al.*, 2009b].

[38] The combination of both astronomical tidal and surge components defines the overall variation of extreme sea levels within a year. After the stepwise analysis, about 90% of the sea level records in the analyzed stations successfully fit a seasonal model composed of an annual and semiannual component in the location parameter and an annual cycle in the scale parameter of the GEVD. The incorporation of seasonal dependence into the extreme model has the advantage of allowing the assessment of return level values on a seasonal or monthly scale. Therefore, we are able to assess the time of the maximum probability of occurrence of an extreme event within a year.

[39] Figure 4a shows the spatial distribution of the month which presents the greatest probability of a high water level value. These results are for the total elevations. Therefore, they may be influenced by local factors such as river runoff and interactions between tide and surge due to shallow waters. However, they are of primary interest in the assessment of flooding risk. The assessment is made by estimating the timing of the largest 50 year return values within a year. The spatial coherence in the results between the studied stations indicates the good quality of the data set.

[40] A clear winter pattern for high water levels is found along European and North American coasts. The maximum probability of high water levels is found to be in the middle of the winter season in northern Europe. Instead, the western European coast (United Kingdom and the Atlantic coasts of France and Iberia) presents higher probability in the late winter or beginning of spring. A gradual south-north spatial distribution from October (in the Caribbean and Gulf coasts) to January appears in northeast United States and Canada, indicating the change in meteorological dominance from

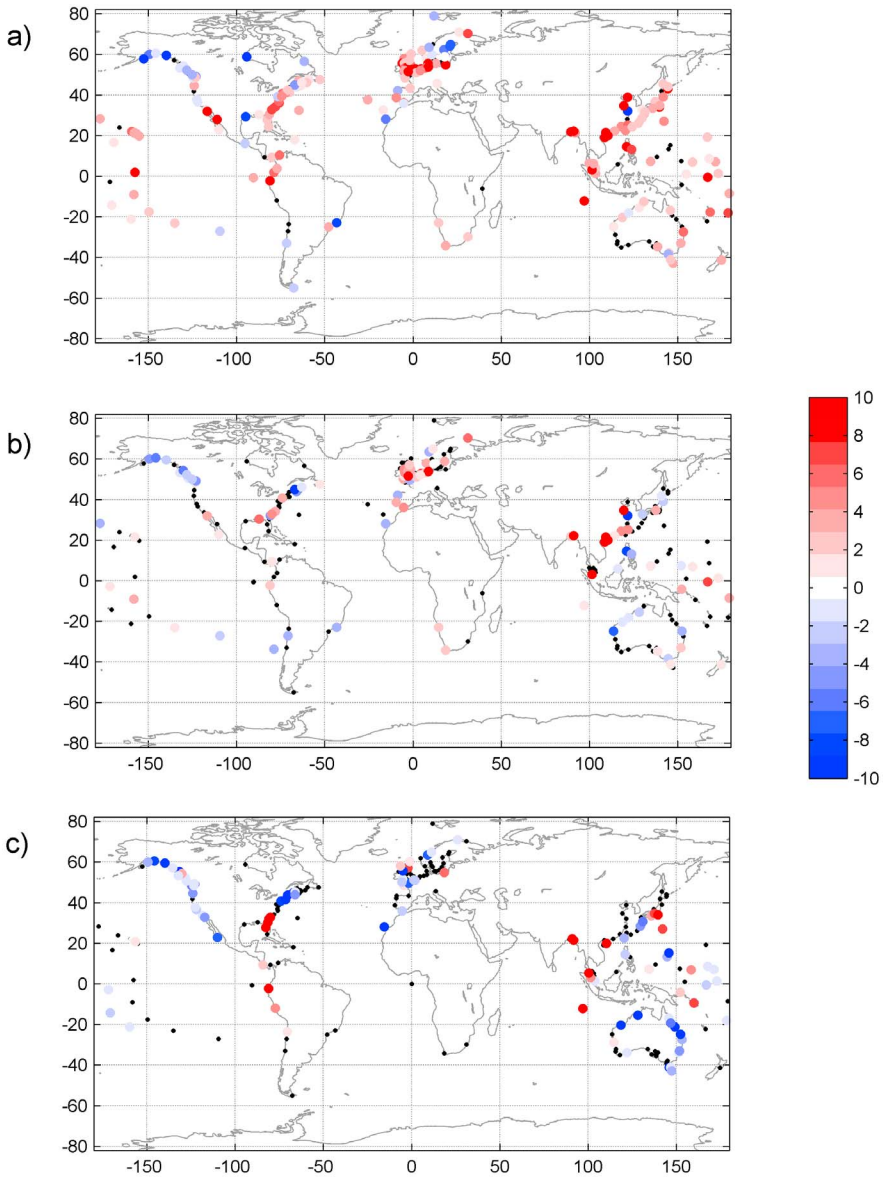

Figure 6. Estimated trends (cm/10 yr) in a 50 year return period of sea level from (a) total elevation, (b) total elevation after removal of annual medians, and (c) 50 year return nontidal residual. Only trends statistically significant at the 95% confidence level are colored.

tropical storms to northeasters [*Zhang et al.*, 2000]. May and June are the more likely months for higher water levels in the south of Australia, April and March are the more likely months for higher water levels in the northwest of Australia, and February and January are the more likely months for higher water levels in the northeast. Japanese and Chinese coasts show extreme water levels during the months from July to September, when typhoons propagate west across the Pacific Ocean. A maximum probability of high water levels is found in August for the Bangladesh coast, as might be expected from the monsoon season.

[41] Figure 4b shows the month of higher probability for an extreme nontidal residual. A spatial seasonal pattern of storminess is observed throughout the winter season in high latitudes (December–January for North America and Europe and June–July south of 20°S), and the September storm surges caused by typhoons in the western Pacific can be observed. The relative importance of nontidal residual to extreme high water levels can be observed in the differences between Figures 4a and 4b. The different months in western Europe, the central and south Pacific, the American coast, and northwest Australia suggest tidal dominance in extreme sea level events in these areas.

4.2. Long-Term Trends

[42] We have made use of different methods to validate the estimations of trends in extreme high waters events. A preliminary analysis of the trends in the high percentiles of the hourly time series from 1970 onward was developed following a similar procedure to that reported by *Woodworth and Blackman* [2004]. Years of data with less than 75% of hourly values were rejected. Trends in the 99

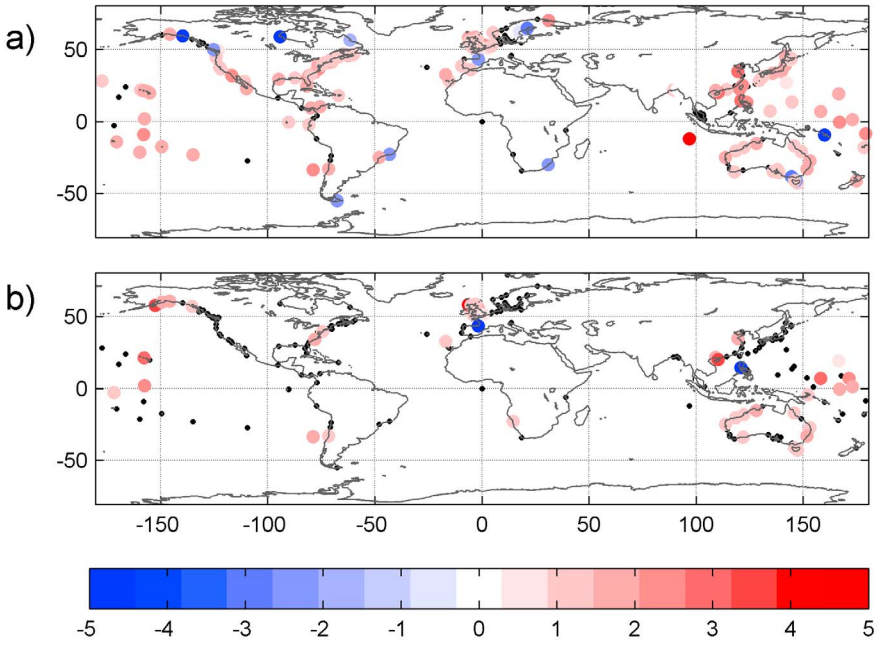

Figure 7. (a) Estimated changes in the frequency of extreme sea level events for the total elevation time series and (b) for the time series with the annual median removed. Changes are the annual percentage of increase/decrease in the occurrence of extreme events relative to the average occurrence rate. Black dots indicate trends with a level of significance below 5%.

percentile of the total elevations and in the corresponding time series reduced to medians were computed using linear regression with allowance for a perigean component. In addition, trends in the same percentiles for the surge component were computed using linear regression (Figure 5).

[43] Regarding the GEVD model, once the best model for parameterizing the seasonal dependence of MM has been obtained, the long-term trends of the extreme high waters or surges can be analyzed. The estimation of long-term trends is computed with allowance for trends in the location and scale parameters of the GEVD, as described above. In the cases that the trends in the location or the scale parameter are statistically significant, the trends in the estimated quantile of the 50 year return periods are computed (Figure 6).

[44] Figure 6a shows the estimated trend of the 50 year return high water level for total sea level observations since 1970. A spatial coherence in the trend gives confidence in the analysis and in the general data quality, even though some local behavior is apparent. A general increase is observed for the majority of the stations at our disposal. This supports the assertions that extreme high-water levels have increased worldwide in recent decades. Pertinent positive trends are found in the North Sea [*Langenberg et al.*, 1999], the east coast of the United States [*Zhang et al.*, 2000], and the west and central Pacific. In contrast, a negative trend is detected in the Arctic and Alaskan parts of northern America [*Larsen et al.*, 2003] and Scandinavia.

[45] A plot of the trends in the 50 year return level quantile from the MM_R is shown in Figure 6b. Most of the positive trends disappear when the MSL variations are removed from the extreme values. This implies that the general world increase in extreme high water levels is due to changes in MSL rather than in storminess. Even so, increases in extremes remain in the North Sea and monsoonal regions (the Bay of Bengal, Malaysia, and the South China Sea). A decrease in extreme high water levels also appears along the northwest coast of Australia.

[46] A generally similar spatial distribution of trends was found for the high percentile and GEVD methods along the world coastline (Figures 5 and 6), although differences were found for the estimated trends of the MM_R in Europe and the western Pacific. These differences may be attributed to the different analyzed values (i.e., 99th percentile rather than true extreme) and methodology (i.e., linear regression rather than extreme value analysis based on maximum likelihood).

[47] The increase or decrease in the rate of occurrence of extreme sea level events was estimated by a nonhomogeneous Poisson process in a complementary analysis. The frequency model was applied to the extreme events of total sea level and annual median reduced sea level during the period of 1970 onward and considers a time-dependent occurrence rate with allowance for the annual cycle, the perigean component, the nodal component, and long-term trends.

[48] In a complementary set of findings to those reported above for Figures 5 and 6, a general increase in occurrence of extreme sea level events is observed in the majority of the stations (Figure 7a). Results for the annual median reduced sea level time series contain a much reduced number of significant trends, as is to be expected if the number of exceedances over threshold are due to the MSL variations (Figure 7b), while small increases occur along the coasts of Australia, the west Pacific, Alaska, and United Kingdom.

[49] In order to obtain information on extreme sea level variability on longer timescales, trends in the longer records

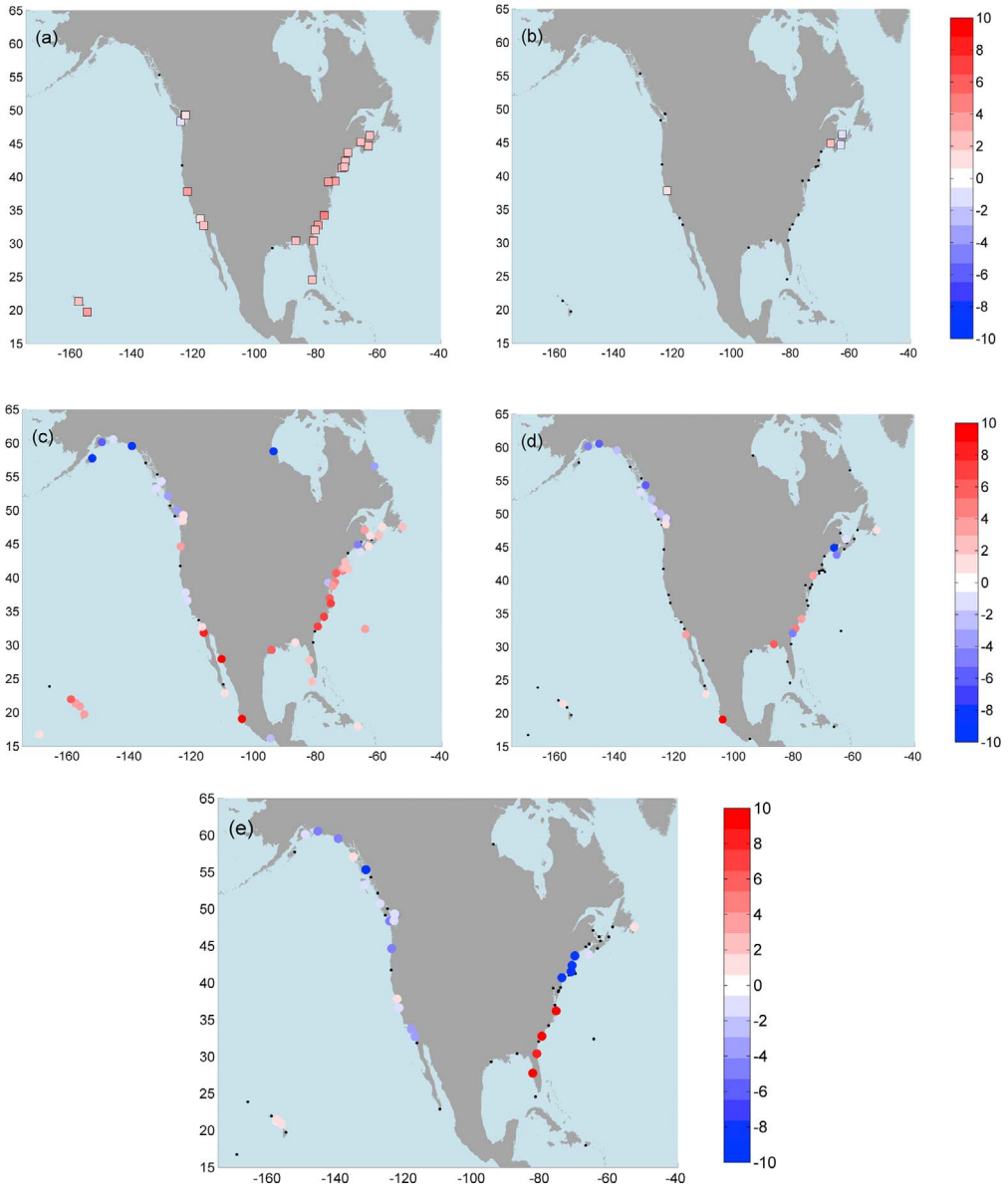

Figure 8. (a) Estimated trends (cm/10 yr) in 50 year return sea level for the total elevation during the last century, (b) same as Figure 8a but with the monthly maxima series reduced to annual median, (c) estimated trends in the 50 year return sea level for recent decades, (d) same as Figure 8c but with the monthly maxima series reduced to the annual median, and (e) trends in the 50 year return nontidal residual since 1970. Only trends statistically significant at the 95% confidence level are colored.

of the data set have been computed separately with the same GEVD method described above. We restricted ourselves to 60 years or more of good quality data, with the result that we were only able to estimate long-term trends for the coasts of the United States, Europe, and south of Australia (red squares in Figure 1).

[50] The estimated trends in North America are displayed in Figure 8. Extreme value analysis of the long records confirms the secular increase on high waters along the U. S. east coast (Figure 8a), although it can be seen that this red grouping disappears for the MM_R analysis (Figures 8b and 8d). A negative trend along the Gulf of Alaska and the northern U. S. Atlantic coast of the nontidal residual (Figure 8e) indicates a reduction of storm activity on these areas in recent decades [e.g., *Bernier and Thompson*, 2006].

[51] Figure 9 shows estimated trends for tide gauges around Europe. Results for the total elevation since 1970 (Figure 9c) show an increase in extreme high water levels in northwest Europe, but that increase does not apply for the whole century (Figure 9a). The only common trends between the analysis for the last century and those for recent decades are decreases in the Baltic Sea, although they completely disappear after the annual median subtraction, suggesting vertical crustal motion as the main cause. The

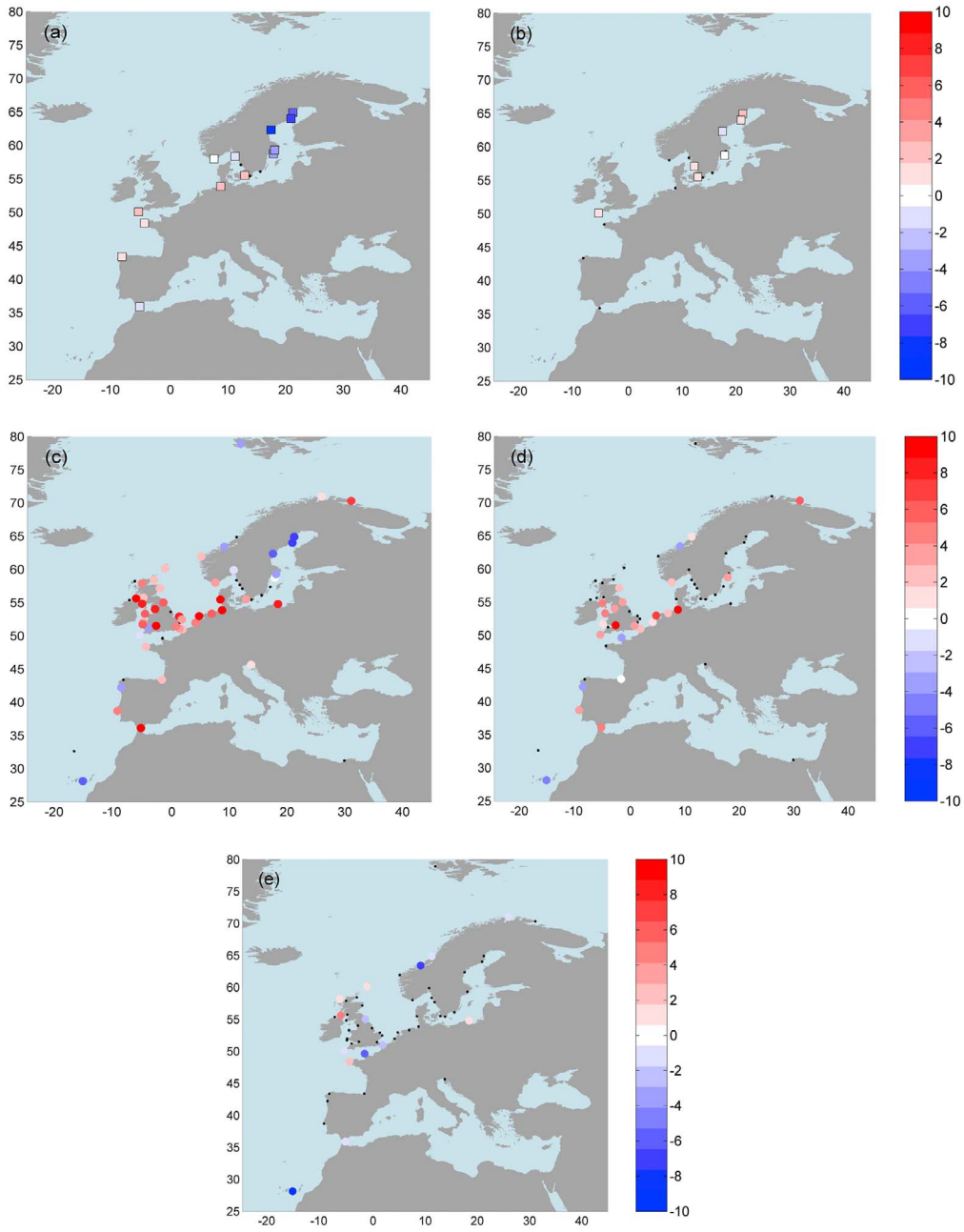

Figure 9. (a) Estimated trends (cm/10 yr) in the 50 year return sea levels for the total elevation during the last century, (b) similar distribution to Figure 9a but with the annual median removed, (c) estimated trends in the 50 year return sea level for recent decades, (d) similar to Figure 9c but with the annual median removed, and (e) trends in the 50 year return nontidal residual since 1970. Only trends significant at the 95% confidence level are colored.

increase in extreme sea levels since 1970, still seen in the maximum values after median subtraction (Figure 9d), is greater in the southern part of the North Sea and on the west coast of the United Kingdom. This may represent an increment in the extent of the climate forcing that causes the higher water levels during recent decades. The analysis of trends in the nontidal residual since 1970 shows only a few sites with statistically significant trends (Figure 9e), which may indicate no increase in the storminess.

4.3. Interannual Variability

[52] The presence of interannual and decadal variations is commonplace in extreme sea level and surge records. The removal of the annual median in sea level subtracts much of the interannual variability that is responsible for changes in MSL. However, high water levels can also include long-period tidal components that are not represented in the MSL time series. For example, the perigean influence is evident in the highest percentile series for the Tuvalu tide gauge

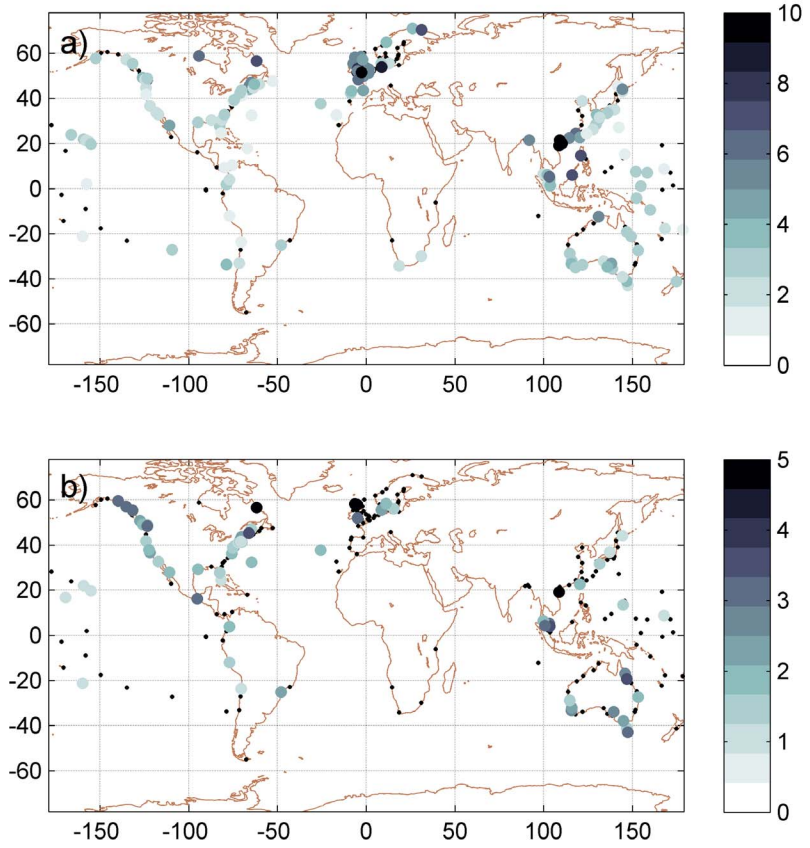

Figure 10. Amplitude (cm) of the (a) nodal cycle and the (b) quasi 4.4 year periodic perigean influence. Black dots show tide fluctuations with a confidence level below 90%.

[*Woodworth and Blackman*, 2004]. In order to evaluate the role of these fluctuations in the extreme sea levels, the sensitivities of the nodal and perigean cycles have been computed for the MM_R (Figure 10). In the present GEVD analysis, the perigean influence was found to be statistically significant in North America, the South China Sea, and at several locations in the east and south of Australia, although with an amplitude of less than 3 cm (Figure 10b). Signals for the nodal component were found to be significant, with amplitudes of up to 5 cm in the northeast Atlantic and the South China Sea (Figure 10a). We note the limitations of obtaining nodal findings from only two cycles of data in the records commencing in 1970.

[53] The impact of the climate indices described above has also been computed. The extreme model with the inclusion of climate index terms was applied to the MM of three variables: total sea level elevations, sea levels with the annual median subtracted, and nontidal residuals. Figure 11a shows the sites for which the MM water levels are affected by ENSO. The sites for significance above the 95% confidence level in the β_{CI} parameter are shown. Results verify the association between the ENSO and the interannual sea level variability along the whole west coast of America and the western tropical Pacific. The propagation of the ENSO signal into the Indian Ocean through the Indonesian throughflow can be seen along the west and south coasts of Australia. The positive relationship along the west coast of the United States indicates a higher probability of a high water level during intense ENSO events. By contrast, the tropical west Pacific and the coast of Australia show sensitivity with reverse sign. Therefore, high sea levels are more probable in those areas during La Niña events [*Feng et al.*, 2004]. The relationship is still significant along the west American coast and the western Pacific basin for the MM_R, but it is reduced by a factor of one half (not shown). This is to be expected, since much of the lower frequency behavior of the ENSO-related sea level variability will have been removed by the annual median subtraction. Results for the extreme nontidal residual show a stronger effect in the tropical Pacific, the southwest American coast, the northwest Atlantic, and western Australia (Figure 11b).

[54] The AO shows the second dominant large-scale climate. Positive significant relations are obtained for the northern European stations, but a negative relation is also detected in southern Europe and the northwest Atlantic. The IOD shows a similar result for extreme water levels, as for Niño3 in the Southern Hemisphere and higher sensitivities for the Bay of Bengal sites. However, no significant relationships are found for MM_R total elevations and nontidal residuals. The AAO and PNA indices have no significant relationships in the extremes of any analyzed tide gauge.

[55] The AO, NAO, EA, EAWR, and SCA indices have an important impact on the variability of the extreme sea

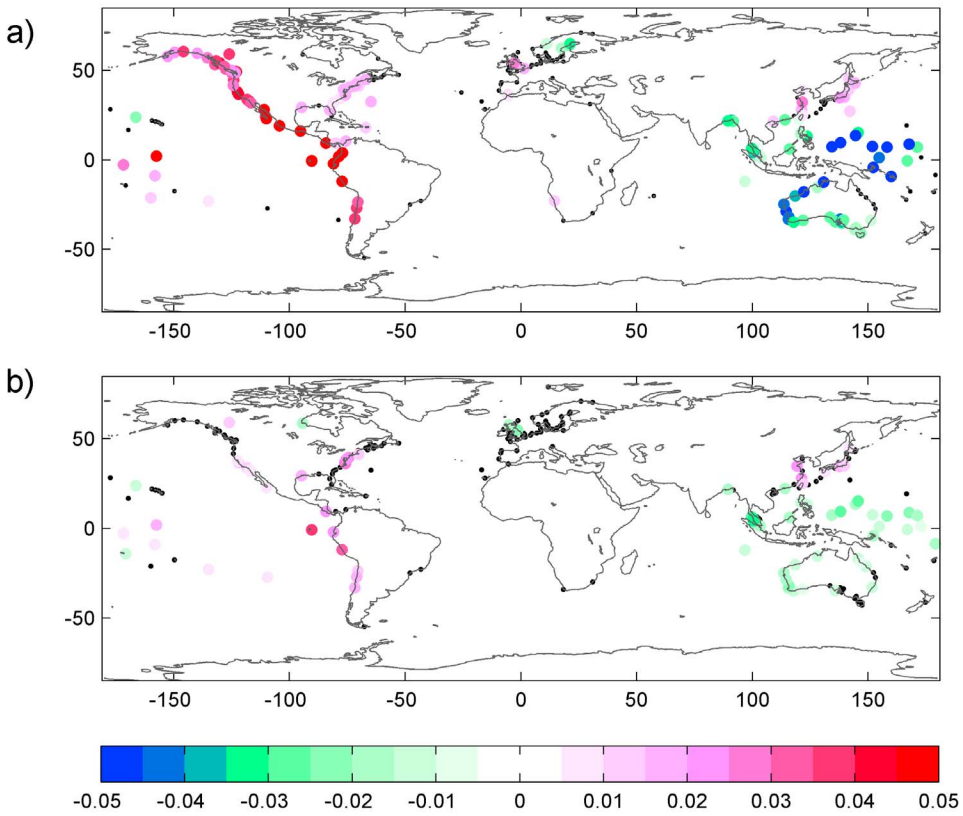

Figure 11. (a) Sensitivity of change in extreme sea levels to the Niño3 index (m/unit index) and (b) corresponding sensitivity in extreme nontidal residual. Only statistically significant relations at the 95% confidence level are colored.

levels along the European coast. Apart from the EAWR index, results for extremes in total sea level, annual median reduced sea level, and nontidal residual provide similar spatial results. This demonstrates that the same climate dynamics are affecting the climate variability of MSL, the extreme sea levels, and storminess in Europe. Figure 12 shows a set of maps of the most significant climate indices for MM_R in the European region. Results for the NAO index show a similar spatial pattern as for the AO, with higher statistical relationships for the northern European stations. The EA index has the highest values of the estimated parameter β_{CI} on the west coast of the United Kingdom, while the SCA index presents dipole sensitivity between southwest Europe and Scandinavia.

5. Conclusions

[56] A data set of 258 hourly sea level records from tide gauges has been used to investigate the spatial and temporal variabilities of extreme high water levels worldwide. The statistical extreme value approach applied to both the total elevations and to the nontidal residuals provides quantitative measures of change in extreme sea level events.

[57] Analysis of seasonal variations shows that they play an important role in the occurrence and magnitude of extreme sea levels. The combination of spring tides and storm surges determine the amplitude and month within a year of higher probability for an extreme sea level event, which may be useful information for coastal management. Results demonstrate that the month with the greatest extreme is not always in the middle of the winter season.

[58] Pronounced trends in recent decades have been found to be prominent features of the extreme sea level distribution along the global coastline. Our present analysis confirms that there has indeed been an increase in extreme high water levels worldwide since 1970. In order to study whether the observed changes of extreme high waters are due to factors other than the generally underlying MSL rise, analyses were made with the annual median sea level removed from the extremes. Results show that the MSL rise is the major reason for the rise in extreme high water at most stations.

[59] Our study, within the limitations of the small number of long records available, indicates that, in general, there was a greater rate of increase in high water levels in recent decades than for the 20th century overall. This finding demonstrates the importance of consideration of decadal variations and accelerations in extremes similar to those in mean sea levels [e.g. *Church and White*, 2006].

[60] Prominent positive trends are detected in the tropical Pacific and monsoonal regions. The negative trends in extreme sea levels observed in the Gulf of Alaska and the Baltic Sea could be due to crustal uplift in those regions [e.g., *Larsen et al.*, 2003]. The estimated increases in high water levels of the east coast of the United States, reported in

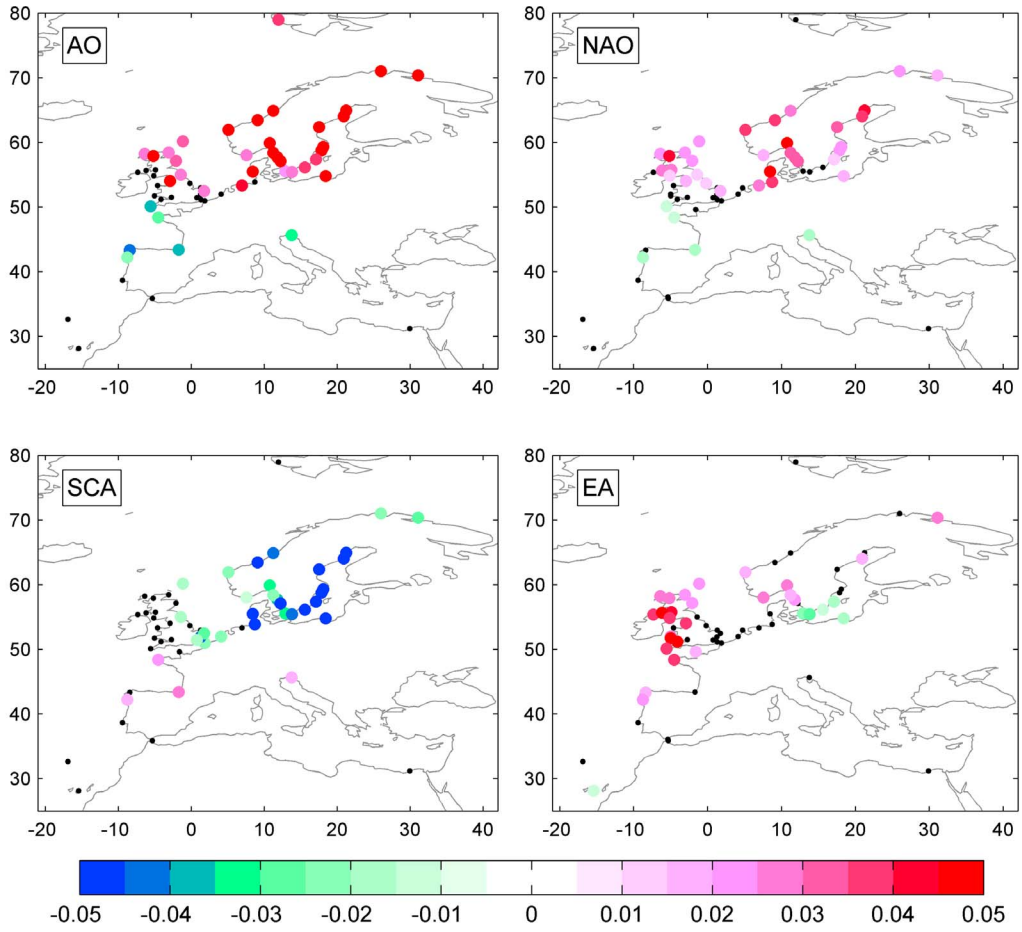

Figure 12. Sensitivity of change in extreme annual median reduced high waters and a set of regional climate indices: Arctic Oscillation (AO), North Atlantic Oscillation (NAO), Scandinavian index (SCA), and East Atlantic Oscillation (EA) (m/unit index).

the present study for recent decades, are consistent with earlier research [*Zhang et al.*, 2000]. The positive trends along the east coast of the United States in observed extreme sea levels have persisted throughout the last century. However, once again, significant trends are not found for the same extreme sea levels with the annual median reduced. The maximum surges show a decrease in the northern part of the coast and an increase on the Gulf Coast. Therefore, the effect of the mean sea level rise over the last century has been a major factor on the impact of storm surges, causing an increase of higher waters levels.

[61] The European Atlantic coast is one of the regions with the highest sea level variations, with tidal ranges from 3 m to more than 10 m and with storm surges, on occasion, of over a meter. Significant positive trends were computed for recent decades in extreme values of total elevation. Nevertheless, there were no significant trends in storm surge levels, indicating that changes in extreme sea level events are caused by natural climate fluctuations in storminess together with changes in the MSL.

[62] The interannual fluctuations in extreme values have been shown to be related to changes in regional climate patterns. An important impact of the El Niño phenomenon has been found throughout the Pacific Ocean and the monsoonal region, while the apparent increase of high water levels in Europe may be governed to some extent by the ocean-atmosphere circulation patterns. El Niño is revealed to be one of the most important forcings responsible for the interannual fluctuations of the extreme sea levels, and these interannual-to-decadal variations will have played a role in the trends computed in extreme sea levels for 1970 onwards. Meanwhile, the impact of astronomical tidal contributions to the extreme sea levels has been found especially significant along the northern American coast, northwestern Europe, the South China Sea, and Australia.

[63] We must state that the present study forms only the first of what we hope will eventually be a considerably expanded GESLA data set which we intend to compile with the cooperation of sea level agencies. We look forward to learning more about the space and time scales of extreme sea levels with the use of that expanded global data set.

[64] **Acknowledgments.** Melisa Menéndez is indebted to the Spanish Ministry of Science and Innovation for the funding provided for an extended visit to the Proudman Oceanographic Laboratory. The authors thank John Hunter of the ACE CRC for initiating the GESLA activity and for advice on the present project. The work was partially funded by Project "GRACCIE" (CSD2007-00067, CONSOLIDERINGENIO 2010), and "C3E" from the Spanish Ministry of Environment, Rural, and Marine Affairs.

References

Akaike, H. (1973), Information theory and an extension of the maximum likelihood principle, in *Proceedings of the 2nd International Symposium on Information Theory*, edited by B. N. Petrov and F. Csáki, pp. 267–281, Akadémia Kiadó, Budapest.

Araujo, I. B., and D. T. Pugh (2008), Sea levels at Newlyn 1915–2005: Analysis of trends for future flooding risks, *J. Coastal Res.*, *24*(4C), 203–212.

Bernier, N. B., and K. R. Thompson (2006), Predicting the frequency of storm surges and extreme sea levels in the northwest Atlantic, *J. Geophys. Res.*, *111*, C10009, doi:10.1029/2005JC003168.

Bindoff, N., et al. (2007), Observations: Ocean climate change and sea level, in *Climate Change 2007: The Physical Science Basis. Contribution of Working Group 1 to the Fourth Assessment Report of the Intergovernmental Panel on Climate Change*, edited by S. Solomon et al., pp. 385–432, Cambridge Univ. Press, U. K.

Bromirski, P. D., R. E. Flick, and D. R. Cayan (2003), Storminess variability along the California Coast: 1858–2000, *J. Clim.*, *16*, 982–993.

Carter, D. J. T., and P. G. Challenor (1981), Estimating return values of environmental variables, *Q. J. R. Meteorol. Soc.*, *107*, 259–266.

Castillo, E., A. S. Hadi, N. Balakrishnan, and J. M. Sarabia (2005), *Extreme Value and Related Models with Applications in Engineering and Science*, Wiley-Interscience, Hoboken, N. J.

Church, J. A., and N. J. White (2006), A 20th century acceleration in global sea level rise, *Geophys. Res. Lett.*, *33*, L01602, doi:10.1029/2005GL024826.

Church, J. A., J. R. Hunter, K. McInnes, and N. J. White (2006), Sea-level rise around the Australian coastline and the changing frequency of extreme events, *Aust. Meteorol. Mag.*, *27* (Nov./Dec.), 19–22.

Coles, S. G. (2001), *An Introduction to Statistical Modelling of Extreme Values*, 208 pp., Springer, London.

Feng, M, Y. Li, and G. Meyers (2004), Multidecadal variations of Fremantle sea level: Footprint of climate variability in the tropical Pacific, *Geophys. Res. Lett.*, *31*, L16302, doi:10.1029/2004GL019947.

Horsburgh, K. J., and C. Wilson (2007), Tide-surge interaction and its role in the distribution of surge residuals in the North Sea, *J. Geophys. Res.*, *112*, C08003, doi:10.1029/2006JC004033.

Jones, P. D., T. Jónsson, and D. Wheeler (1997), Extension to the North Atlantic oscillation using early instrumental pressure observations from Gibraltar and south-west Iceland, *Int. J. Climatol. 17*, 1433–1450.

Kang, S. K., J. Y. Cherniawsky, M. G. G. Foreman, J.-K. So, and S. R. Lee (2008), Spatial variability in annual sea level variations around the Korean peninsula, *Geophys. Res. Lett.*, *35*, L03603, doi:10.1029/2007GL032527.

Katz, R. W., M. B. Parlange, and P. Naveau (2002), Statistics of extremes in hydrology, *Adv. Water Resour.*, *25*(8–12), 1287–1304.

Langenberg, H., A. Pfizenmayer, H. von Storch, and J. Sündermann (1999), Storm related sea level variations along the North Sea coast: Natural variability and anthropogenic change, *Cont. Shelf Res.*, *99*, 821–842.

Larsen, C. F., K. A. Echelmeyer, J. T. Freymueller, and R. J. Motyka (2003), Tide gauge records of uplift along the northern Pacific-North American plate boundary, 1937 to 2001, *J. Geophys. Res.*, *108*(B4), 2216, doi:10.1029/2001JB001685.

Lowe, J. A., J. M. Gregory, and R. A. Flather (2001), Changes in the occurrence of storm surges around the United Kingdom under a future climate scenario using a dynamic storm surge model driven by the Hadley Centre climate models, *Clim. Dyn.*, *18*, 179–188.

Lowe, J. A., et al. (2010), Past and future changes in extreme sea levels and waves, in *Understanding Sea-Level Rise and Variability*, edited by J. A. Church et al., Blackwell, Hoboken, N. J.

Marcos, M., M. N. Tsimplis, and A. G. P. Shaw (2009), Sea level extremes in the southern Europe, *J. Geophys. Res.*, *114*, C01007, doi: 10.1029/2008JC004912.

Méndez, F. J., M. Menéndez, A. Luceño, and I. J. Losada (2007), Analyzing monthly extreme sea levels with a time-dependent GEV model, *J. Atmos. Oceanic Technol.*, *24*, 894–911.

Menéndez, M., F. J. Méndez, C. Izaguirre, A. Luceño, and I. J. Losada (2009a), The influence of seasonality on estimating return values of significant wave height, *Coastal Eng.*, *56*(3), 211–219.

Menéndez, M., F. J. Méndez, and I. J. Losada (2009b), Forecasting seasonal to interannual variability in extreme sea levels, *ICES J. Mar. Sci.*, *66*(7), 1490–1496, doi:10.1093/icesjms/fsp095.

Peltier, W. R. (2001), Global glacial isostatic adjustment and modern instrumental records of relative sea level history, in *Sea Level Rise: History and Consequences*, edited by B. C. Douglas, M. S. Kearney, and S. P. Leatherman, pp. 61–95, Academic, New York.

Pickands, J. (1975), Statistical inference using extreme order statistics, *Ann. Stat. 3*, 119–131.

Pugh, D. T. (1987), *Tides, Surges and Mean Sea Level: A Handbook for Engineers and Scientists*, 472 pp., Wiley, Chichester, U. K.

Pugh, D. T., and G. A. Maul (1999) Coastal sea level prediction for climate change, in *Coastal Ocean Prediction*: *Coastal and Estuaries Studies*, edited by C. N. K. Mooers, 377-404, AGU, Washington, D. C.

Raicich, F. (2003), Recent evolution of sea-level extremes at Triestre (Northern Adriatic), *Cont. Shelf Res.*, *23*(3), 225–235.

Singh, O. P. (2001), Cause-effect relationships between sea surface temperature, precipitation and sea level along the Bangladesh coast, *Theor. Appl. Clim.*, *68*, 233–243.

Tsimplis, M. N., and P. L. Woodworth (1994), The global distribution of the seasonal sea level cycle calculated from coastal tide gauge data, *J. Geophys. Res.*, *99*, 16,031–16,039.

Wang, J., and X. Zhang (2008), Downscaling and projection of winter extreme daily precipitation over North America, *J. Clim.*, *21*(5), 923–937.

Woodworth, P. L., and D. L. Blackman (2002), Changes in extreme high waters at Liverpool since 1768, *Int. J. Climatol.*, *22*, 697–714.

Woodworth, P. L., and D. L. Blackman (2004), Evidence for systematic changes in extreme high waters since the mid-1970s, *J. Clim.*, *17*, 1190–1197

Zhang, K., B. C. Douglas, and S. P. Leatherman (2000), Twentieth-century storm activity along the U.S. east coast, *J. Clim.*, *13*, 1748–1761.

M. Menéndez, Environmental Hydraulic Institute, E.T.S. Ingenieros de Caminos, Canales y Puertos, Universidad de Cantabria, Avda. de los Castros s/n, E-39005 Santander, Spain. (menendezm@unican.es)

P. L. Woodworth, Proudman Oceanographic Laboratory, Jason Proudman Building, 6 Brownlow St., Liverpool L3 5DA, UK.